

## VLBA Astrometry of the Fastest-spinning Magnetar Swift J1818.0–1607: A Large Trigonometric Distance & A Small Transverse Velocity

HAO DING <sup>1,\*</sup> MARCUS E. LOWER <sup>2</sup> ADAM T. DELLER <sup>3,4</sup> RYAN M. SHANNON <sup>3,4</sup> FERNANDO CAMILO <sup>5</sup> AND  
JOHN SARKISSIAN<sup>6</sup>

<sup>1</sup>Mizusawa VLBI Observatory, National Astronomical Observatory of Japan, 2-12 Hoshigaoka, Mizusawa, Oshu, Iwate 023-0861, Japan

<sup>2</sup>Australia Telescope National Facility, CSIRO, Space and Astronomy, PO Box 76, Epping, NSW 1710, Australia

<sup>3</sup>Centre for Astrophysics and Supercomputing, Swinburne University of Technology, John St., Hawthorn, VIC 3122, Australia

<sup>4</sup>ARC Centre of Excellence for Gravitational Wave Discovery (OzGrav), Australia

<sup>5</sup>South African Radio Astronomy Observatory, 2 Fir Street, Observatory 7925, South Africa

<sup>6</sup>Australia Telescope National Facility, CSIRO, Space and Astronomy, Parkes Observatory, PO Box 276, Parkes NSW 2870, Australia

### ABSTRACT

In addition to being the most magnetic objects in the known universe, magnetars are the only objects observed to generate fast-radio-burst-like emissions. The formation mechanism of magnetars is still highly debated, and may potentially be probed with the magnetar velocity distribution. We carried out a 3-year-long astrometric campaign on Swift J1818.0–1607 — the fastest-spinning magnetar, using the Very Long Baseline Array. After applying the phase-calibrating 1D interpolation strategy, we obtained a small proper motion of  $8.5 \text{ mas yr}^{-1}$  magnitude, and a parallax of  $0.12 \pm 0.02 \text{ mas}$  (uncertainties at  $1\sigma$  confidence throughout the Letter) for Swift J1818.0–1607. The latter is the second magnetar parallax, and is among the smallest neutron star parallaxes ever determined. From the parallax, we derived the distance  $9.4_{-1.6}^{+2.0} \text{ kpc}$ , which locates Swift J1818.0–1607 at the far side of the Galactic central region. Combined with the distance, the small proper motion leads to a transverse peculiar velocity  $v_{\perp} = 48_{-16}^{+50} \text{ km s}^{-1}$  — a new lower limit to magnetar  $v_{\perp}$ . Incorporating previous  $v_{\perp}$  estimates of seven other magnetars, we acquired  $v_{\perp} = 149_{-68}^{+132} \text{ km s}^{-1}$  for the sample of astrometrically studied magnetars, corresponding to the three-dimensional space velocity  $\sim 190_{-87}^{+168} \text{ km s}^{-1}$ , smaller than the average level of young pulsars. Additionally, we found that the magnetar velocity sample does not follow the unimodal young pulsar velocity distribution reported by Hobbs et al. at  $> 2\sigma$  confidence, while loosely agreeing with more recent bimodal young pulsar velocity distributions derived from relatively small samples of quality astrometric determinations.

*Keywords:* Very long baseline interferometry (1769) — Magnetars (992) — Radio pulsars (1353) — Proper motions (1295) — Annual parallax (42)

### 1. INTRODUCTION

Magnetars are a class of highly magnetized, slowly rotating neutron stars with surface magnetic field strengths typically inferred in the range  $10^{14} - 10^{15} \text{ G}$ , making them the most magnetic objects in the known universe. They have been observed to emit an enormous amount of high-energy electromagnetic radiation, and to undergo powerful X-ray and gamma-ray outbursts. The high energy emission from these objects is thought to be

powered by the decay of their powerful magnetic fields (Thompson & Duncan 1995; Heyl & Kulkarni 1998). A radio burst with a luminosity approaching those of fast radio bursts (FRBs) was observed from the Galactic magnetar SGR 1935+2154 (Andersen et al. 2020; Bochenek et al. 2020), which strongly reinforced the long-held speculation that a fraction (if not all) of FRBs originate from magnetars.

At the basis, the formation mechanism of magnetars is still under debate. A few theories have been proposed to explain the origin of magnetars, including core-collapse supernovae (CCSNe) (Schneider et al. 2019; Shenar et al. 2023), accretion-induced collapse (AIC) of white dwarfs

hdingastro@hotmail.com

\* EACOA Fellow

(Lipunov & Postnov 1985; Fryer et al. 1999; Dessart et al. 2007; Margalit et al. 2019; Ruiter et al. 2019) and double neutron star (DNS) mergers (Giacomazzo & Perna 2013; Margalit et al. 2019). The light curves of a few X-ray transients are believed to be generated by extragalactic millisecond magnetars born from neutron star mergers (e.g. Xue et al. 2019; Sun et al. 2019; Ai & Zhang 2021). Despite these evidences in favour of magnetar production in mergers, the DNS-merger scenario is disfavored for the bulk of the known Galactic magnetar population by their low Galactic latitudes (Olausen & Kaspi 2014). On the other hand, at least a fraction of Galactic magnetars are expected to come from CC-SNe, given the 15 confirmed or proposed associations (see Table 1 of Sherman et al. 2024) between Galactic magnetars and supernova remnants (SNRs) (e.g. Vasisht & Gotthelf 1997; Klose et al. 2004; Gelfand & Gaensler 2007; Gaensler & Chatterjee 2008; Gaensler 2014; Borkowski & Reynolds 2017; Bailes et al. 2021). For formation channels other than the CCSNe or the DNS-merger channel, it remains unclear whether they would contribute to the birth of Galactic magnetars. As the magnetar space (or peculiar) velocity (i.e., velocity with respect to its neighbourhood in the Galaxy) distribution probably varies with the underlying formation channel, it can be used to probe the formation mechanism of Galactic magnetars (Ding 2022; Ding et al. 2023a), with an increasing number of astrometrically constrained magnetars. In addition, pinpointing the 3D locations of magnetars in our Galaxy can help develop a template for magnetar distribution in spiral galaxies; this template can be compared against FRBs localized to spiral galaxy hosts (Mannings et al. 2021), thus testing the link between FRBs and magnetars (Ding 2022).

To date, approximately 24 magnetars and 6 magnetar candidates have been discovered<sup>1</sup>; however, only 6 (including Swift J1818.0–1607) have been found to be radio bright. Observations of magnetar radio pulses reveal they are quite distinct from the radio emission seen in pulsars – they have largely flat radio spectra and their pulse profiles are highly variable on timescales ranging between seconds to years (e.g. Camilo et al. 2008; Lower et al. 2020b). With a current sample size of only eight magnetars with proper motions well measured at radio (Deller et al. 2012; Bower et al. 2015; Ding et al. 2020c) or infrared/optical wavelengths (Tendulkar et al. 2012, 2013; Lyman et al. 2022), the appearance of a new radio-emitting magnetar offers a valuable opportunity

for study, particularly for pulsar timing and astrometry, both of which can be performed much more precisely with radio observations than with optical/infrared or X-rays (e.g. Kaplan et al. 2008). Moreover, the high spatial resolution promised by radio interferometry would reduce the sample bias that favors magnetars with larger proper motions. It is also noteworthy that timing observations of a magnetar can, in principle, acquire position and proper motion measurements as well. However, such measurements are hampered by the extreme torque variations and associated spin-down noise of magnetars (e.g. Camilo et al. 2007). Hence, adopting the accurate interferometry-based position, proper motion and parallax would significantly improve the reliability and usefulness of timing observations of radio magnetars.

### 1.1. *Swift* J1818.0–1607

Swift J1818.0–1607 was detected by Swift/BAT (Burst Alert Telescope) and reported on 12 March 2020 as a new soft gamma-ray repeater (SGR) and a magnetar candidate<sup>2</sup>. Its identity as a magnetar was soon confirmed by the NICER team with follow-up observations (Enoto et al. 2020). Subsequently, pulsed radio emission at  $\approx 0.7$  mJy was detected at L band with the Effelsberg and Lovell telescopes respectively (Champion et al. 2020), showing a high dispersion measure (DM) of  $706 \text{ pc cm}^{-3}$ . The distance to Swift J1818.0–1607 based on the DM is estimated to be 4.8 to 8.1 kpc (Lower et al. 2020b), according to the YMW16 (Yao et al. 2017) and the NE2001 (Cordes & Lazio 2002) models of the Galactic free electron distribution. The radio emission of Swift J1818.0–1607 was initially found to be steep-spectrum (spectral index  $\alpha \lesssim -1.8$ , e.g. Lower et al. 2020b; Champion et al. 2020), which then flattened sometime in July 2020 at cm- to sub-mm-wavelengths (e.g. Lower et al. 2020a; Torne et al. 2020). Combining the spin period and its time derivative obtained with pulsar timing, Rajwade et al. (2022) derived a characteristic age of  $\sim 860$  yr, potentially making Swift J1818.0–1607 the youngest known magnetar to date.

The discovery of this new radio-loud magnetar offers a rare chance to refine the magnetar space velocity distribution. To obtain reliable space velocity for Swift J1818.0–1607 requires determination of both its proper motion and distance, which can potentially be obtained with very long baseline interferometry (VLBI) observations. In this Letter, we introduce the results of our 3-year-long astrometric campaign

<sup>1</sup> As counted by <http://www.physics.mcgill.ca/~pulsar/magnetar/main.html>. The count does not include PSR J1846–0258.

<sup>2</sup> <https://gcn.gsfc.nasa.gov/gcn3/27373.gcn3>

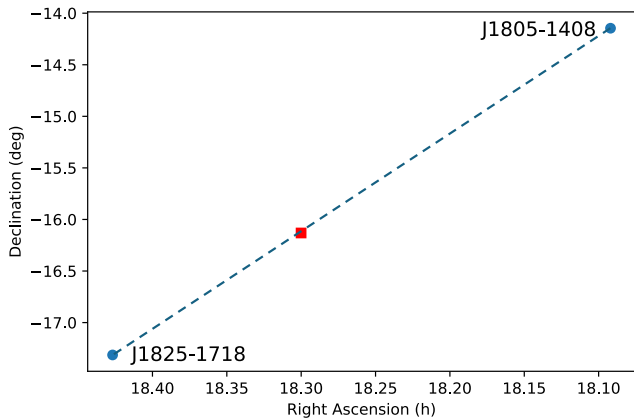


**Figure 1.** Calibrator configuration for the astrometry of Swift J1818.0–1607, where Swift J1818.0–1607 is represented by the red rectangle is phase-referenced to two quasars, ICRF J182536.5–171849 and ICRF J180531.2–140844. The dashed line connects the two quasars, and is only  $25''.7$  away from Swift J1818.0–1607.

of Swift J1818.0–1607, and discuss their implications. Throughout the Letter, uncertainties are given at 68% confidence, unless otherwise stated.

## 2. OBSERVATIONS

Soon after the confirmation of Swift J1818.0–1607 as a new radio magnetar (Champion et al. 2020), we proposed and acquired 3 Director’s Discrepancy Time (DDT) observations from the Very Long Baseline Array (VLBA) under the project code BD232. To suppress the propagation-related systematic errors, the 1D interpolation strategy (e.g. Fomalont & Kopeikin 2003; Doi et al. 2006; Ding et al. 2020c) was adopted in BD232 and the following observations, where Swift J1818.0–1607 is phase-referenced to two quasars (i.e., ICRF J182536.5–171849 and ICRF J180531.2–140844) quasi-colinear with Swift J1818.0–1607 (see Figure 1). Given the then-steep radio spectrum (e.g. Lower et al. 2020b; Champion et al. 2020), the first VLBA observation (project code: BD232A) of Swift J1818.0–1607 was made at  $\sim 1.6$  GHz in April 2020. Unfortunately, no detection was achieved from the first VLBA observation (see Section 3.1 for the likely reason); the  $5\sigma$  upper limit of the BD232A observation is  $0.29 \text{ mJy beam}^{-1}$  (Ding et al. 2020b).

After the spectral flattening of Swift J1818.0–1607 in July 2020, we changed the observing frequency to  $\sim 8.8$  GHz to reduce the effects of angular broadening caused by ionized interstellar media (IISM), and achieved the first VLBI detection of Swift J1818.0–1607 (Ding et al. 2020b). Thereafter, we extended the astrometric campaign with two regular VLBA proposals under the project codes BD241 and BD254, and made in

total 16 VLBA observations. The details of the observations are summarized in Table 1.

Our VLBA campaign of Swift J1818.0–1607 was supported by high-cadence pulsar timing observations of Swift J1818.0–1607 using the Murriyang/Parkes 64-meter radio telescope: ongoing changes in the flux density and pulse ephemeris of Swift J1818.0–1607 were provided from the timing observations. Generally, Swift J1818.0–1607 is a faint target with  $\lesssim 1 \text{ mJy}$  unresolved flux density averaged over the spin period (see Table 1). Based on the pulse ephemerides, pulsar gating was implemented at correlation (of the VLBA data) using the DiFX software correlator (Deller et al. 2011), which typically improves the image S/N of Swift J1818.0–1607 by a factor of  $\sim 2$  (see Table 1).

In addition, the flux density of Swift J1818.0–1607 is highly variable. For instance, the flux density dropped below the detection limit of VLBA between April 2022 and November 2022. In response to the decline of flux density, the data recording rate of the BD254 observations was increased from 2 Gbps to the highest 4 Gbps. As a result, the central observing frequency changes by 0.1 GHz (see Table 1). The resultant position shift of Swift J1818.0–1607 due to the frequency-dependent core shifts (FDCSs; e.g. Sokolovsky et al. 2011) of the phase calibrators is at the order of  $\lesssim 2 \mu\text{as}$ . Therefore, the slightly different central observing frequency in BD254 observations has negligible impact on the astrometric results. In December 2022, the flux density of Swift J1818.0–1607 rebounded, which, however, only lasted for about 3 months. Since early 2023, the flux density of Swift J1818.0–1607 had been declining again (Lower et al. in prep.), then faded below the sensitivity of the VLBA. Consequently, the VLBA observations originally planned for September 2023 were canceled; the final VLBA observations reported in the Letter were made in March 2023.

## 3. DATA REDUCTION & DIRECT RESULTS

We used the `psrvlbireduce`<sup>3</sup> pipeline for the data reduction of the VLBA data. The pipeline is written in `ParselTongue`, an interface connecting AIPS (Greisen 2003) and `python`. As mentioned in Section 2, the 1D interpolation strategy was adopted in the astrometric campaign of Swift J1818.0–1607. Prior to this astrometric campaign, the same strategy has been used in the VLBI astrometry of the radio-loud magnetar XTE J1810–197, which led to the first magnetar parallax (Ding et al. 2020c) (D20). The reduction of the

<sup>3</sup> <https://github.com/dingswin/psrvlbireduce>

**Table 1.** Details of VLBA observations

Project code	yyyy-mm	Central obs. freq. (GHz)	Data rate (Gbps)	Detection?	$\mathcal{S}_{\text{avg}}^a$ (mJy)	Gating gain <sup>b</sup>
BD232A	2020-04	1.6	2	no	—	—
BD232B	2020-08	8.76	2	yes	1.3	— <sup>c</sup>
BD232C	2020-11	8.76/15.24 <sup>d</sup>	2	yes	1.1	1.4
BD241A	2021-03	8.76	2	yes	0.83	2.3
BD241B	2021-03	8.76	2	yes	0.48	2.0
BD241C	2021-09	8.76	2	yes	0.85	1.7
BD241D	2021-10	8.76	2	yes	1.0	1.9
BD241E	2022-03	8.76	2	yes	0.23	1.9
BD241F	2022-04	8.76	2	no	—	—
BD241G	2022-04	8.76	2	no	—	—
BD254A	2022-12	8.63	4	yes	0.36	2.1
BD254B	2022-12	8.63	4	yes	0.49	2.0
BD254C	2023-03	8.63	4	yes	0.33	4.1
BD254D	2023-03	8.63	4	yes	0.44	3.2
BD254E	2023-03	8.63	4	yes	0.25	3.6
BD254F	2023-03	8.63	4	yes	0.26	2.8

<sup>a</sup>  $\mathcal{S}_{\text{avg}}$  stands for the unresolved flux density averaged over the spin period.

<sup>b</sup> The gating gain is the ratio between the gated and the ungated image S/Ns.

<sup>c</sup> The pulsar gating at the BD232B epoch was unsuccessful.

<sup>d</sup> A dual-frequency observation was made to identify the best observing frequency. We eventually gave up observing at 15 GHz due to the absence of suitable calibrator plan.

Swift J1818.0–1607 data follows the same procedure as D20: the wrap of the residual phase between the two phase calibrators was solved in an iterative style; the set of corrections leading to the largest image S/N of the magnetar is adopted as the solution. Compared to D20, acquiring the phase-wrap solutions is straightforward in this campaign, thanks to the higher observing frequency and the smaller angular distance (5°8) between the two phase calibrators. Observing at higher frequency significantly reduces the impact of IISM-induced angular broadening (see Section 3.1). As a result, much better phase solutions were obtained at longer baselines, and no data from any station were excluded from the subsequent analysis. The image models of the two phase calibrators are provided online<sup>4</sup>, in order to convenience the reproduction of our results.

After the data reduction, we detected Swift J1818.0–1607 in 13 of the 16 VLBA observations (see Table 1). From the final image of Swift J1818.0–1607 acquired at each epoch of detection, we obtained one  $\sim 8.7$ -GHz position and its statistical uncertainty  $\sigma_{ij}^{\mathcal{R}}$  (where  $i = \alpha, \delta$  denotes right ascension and declination,  $j = 1, 2, 3, \dots$  indicates differ-

**Table 2.** Position series of Swift J1818.0–1607

Epoch (yr)	Right ascension	Declination
2020.6314	18 <sup>h</sup> 18 <sup>m</sup> 00 <sup>s</sup> .193404(2 5)	−16°07′53″00499(5 15)
2020.8739	18 <sup>h</sup> 18 <sup>m</sup> 00 <sup>s</sup> .193349(3 5)	−16°07′53″00703(9 23)
2021.1906	18 <sup>h</sup> 18 <sup>m</sup> 00 <sup>s</sup> .193285(2 5)	−16°07′53″00930(6 22)
2021.2371	18 <sup>h</sup> 18 <sup>m</sup> 00 <sup>s</sup> .193269(3 5)	−16°07′53″00956(8 14)
2021.6933	18 <sup>h</sup> 18 <sup>m</sup> 00 <sup>s</sup> .193140(2 4)	−16°07′53″01286(6 14)
2021.7780	18 <sup>h</sup> 18 <sup>m</sup> 00 <sup>s</sup> .193126(2 4)	−16°07′53″01394(5 12)
2022.2179	18 <sup>h</sup> 18 <sup>m</sup> 00 <sup>s</sup> .193029(6 7)	−16°07′53″0174(2 2)
2022.9393	18 <sup>h</sup> 18 <sup>m</sup> 00 <sup>s</sup> .192837(3 4)	−16°07′53″02306(8 15)
2022.9420	18 <sup>h</sup> 18 <sup>m</sup> 00 <sup>s</sup> .192837(3 5)	−16°07′53″0227(1 3)
2023.1633	18 <sup>h</sup> 18 <sup>m</sup> 00 <sup>s</sup> .192795(2 5)	−16°07′53″02436(7 22)
2023.2015	18 <sup>h</sup> 18 <sup>m</sup> 00 <sup>s</sup> .192778(3 5)	−16°07′53″02470(8 33)
2023.2261	18 <sup>h</sup> 18 <sup>m</sup> 00 <sup>s</sup> .192786(3 5)	−16°07′53″02475(8 17)
2023.2425	18 <sup>h</sup> 18 <sup>m</sup> 00 <sup>s</sup> .192775(2 4)	−16°07′53″02516(5 12)

The errors on the left and right side of “|” represent, respectively, statistical uncertainty (from the image-plane position fit) and the total uncertainty adding a fiducial systematic component to the statistical component (see Section 4).

<sup>4</sup> available on Zenodo under an open-source Creative Commons Attribution license: [doi:10.5281/zenodo.11239303](https://doi.org/10.5281/zenodo.11239303)

ent epochs) of Swift J1818.0–1607 using JMFIT (of the AIPS package), which is compiled in Table 2.



### 3.1. Angular broadening of Swift J1818.0–1607

From the final images of Swift J1818.0–1607, the apparent size of Swift J1818.0–1607 can also be constrained. Pulsars are point-like sources, so their apparent sizes are normally consistent with zero (e.g. Cordes et al. 1983). The VLBI image of a pulsar only becomes resolved when multi-path propagation of its radio emissions occurs due to scattering by IISM (e.g. Bower et al. 2014; Ding et al. 2023b). By the method described in Appendix A of D20, we estimated a half width  $\theta_{\text{sc}} = 1.08 \pm 0.37$  mas of the angular-broadened size for Swift J1818.0–1607 at  $\sim 8.7$  GHz. As  $\theta_{\text{sc}}$  theoretically changes with the observing frequency  $\nu$  as  $\nu^{-11/5}$  assuming a thin-screen distribution of the foreground IISM (Goodman & Narayan 1989; Macquart & Koay 2013), the  $\theta_{\text{sc}}$  at 1.6 GHz is  $\sim 41.5 \times (1.08 \pm 0.37)$  mas =  $45 \pm 15$  mas. Therefore, the non-detection of the BD232A observation was likely mainly caused by the severe angular broadening at  $\sim 1.6$  GHz.

## 4. SYSTEMATIC ERRORS & ASTROMETRIC INFERENCE

The astrometric parameters, including the reference position, proper motion, and parallax, can be inferred from the position series (see Table 2) of Swift J1818.0–1607. In addition to the statistical positional uncertainties  $\sigma^{\mathcal{R}}$  (i.e., the uncertainties due to random thermal noise in the image) that can be evaluated from the final Swift J1818.0–1607 images, systematic errors mainly caused by atmospheric propagation effects also contribute to the error budget of the Swift J1818.0–1607 positions provided in Table 2. In three different approaches, we carried out astrometric inference that accounts for the presence of systematic errors.

In the first approach, we derived astrometric parameters along with the fiducial systematic uncertainties  $\sigma^{\mathcal{S}}$  using the same least-squares method described in Section 4.2 of D20, except that the coefficient  $A$  in Equation 2 of D20 was directly estimated with respect to the virtual calibrator. We obtained  $A = 6.79 \times 10^{-2}$  for this work. The corresponding total uncertainties calculated as  $\sqrt{(\sigma^{\mathcal{R}})^2 + (\sigma^{\mathcal{S}})^2}$  are dominated by  $\sigma^{\mathcal{S}}$ , and provided on the right side of the “|” marks in Table 2. The resultant astrometric fit is given in Table 3. In the second approach, we performed bootstrap (Efron & Tibshirani 1994) analysis as described in Section 3.1 of D20, based on the error recipe obtained with the first approach. To be independent of the first approach, we also carried out bootstrapping based on only  $\sigma^{\mathcal{R}}$ . The results of the two bootstrap realizations can be found in Table 3.

In the last approach, we made Bayesian astrometric inference using `sterne.py`<sup>5</sup> (Ding & Deller 2024). Following Ding et al. (2023b), we estimated the systematic errors by introducing the correction factor  $\eta_{\text{EFAC}}$  as

$$\sigma_{ij}(\eta_{\text{EFAC}}) = \sqrt{(\sigma_{ij}^{\mathcal{R}})^2 + (\eta_{\text{EFAC}} \cdot \sigma_{ij}^{\mathcal{S}})^2}, \quad (1)$$

where  $i = \alpha, \delta$  denotes right ascension (RA) or declination,  $j = 1, 2, 3, \dots$  indicates different epochs. The results of the Bayesian inference are provided in Table 3. Furthermore, in this work, we introduce an extra nuisance parameter into the Bayesian inference in order to better characterize the systematic errors, which is explained as follows.

### 4.1. Inference of systematics: 2 better than 1

The estimation of  $\sigma_{ij}^{\mathcal{S}}$  based on Equation 2 of D20 assumes  $\sigma_{\alpha j}^{\mathcal{S}}/\sigma_{\delta j}^{\mathcal{S}} = \Theta_{\alpha j}/\Theta_{\delta j}$ , where  $\Theta_{ij}$  refers to the synthesized beam size projected to the  $i$ -th direction. This assumption is not necessarily true. In particular, in low-elevation observations (which is the case for Swift J1818.0–1607 observations with VLBA), any change in the declination of pointing (during the source switches) would cause disproportionately larger path length difference (thus leading to disproportionately larger propagation-related systematics), as compared to any change in the RA of pointing. Therefore, we introduced an extra nuisance parameter  $\eta_{\delta}$  (i.e., EFAD in `sterne.py`), and infer the systematics as

$$\sigma_{ij}(\eta'_i) = \sqrt{(\sigma_{ij}^{\mathcal{R}})^2 + (\eta'_i \cdot \sigma_{ij}^{\mathcal{S}})^2}, \quad (2)$$

where  $\eta'_\alpha = \eta_{\text{EFAC}}$ , and  $\eta'_\delta = \eta_{\text{EFAC}} \cdot \eta_{\delta}$ . When the inference of  $\eta_{\delta}$  is not requested, Equation 2 returns to Equation 1. The results of the Bayesian inference that includes both  $\eta_{\text{EFAC}}$  and  $\eta_{\delta}$  are listed in Table 3. The parallax signature revealed with the two-nuisance-parameter (hereafter abbreviated as 2NP) Bayesian inference is illustrated in Figure 2, where the positional uncertainties are already updated according to Equation 2.

As described in this section, we made astrometric inference that factors in systematic errors by different methods and error recipe. As shown in Table 3, all the methods and the error recipes offer consistent astrometric results. Following the discussion in Section 4.2 of Ding et al. (2023b) based on an astrometric sample of 18, we continue to adopt Bayesian results in this work.

<sup>5</sup> The `sterne.py` version utilized in this work is made publicly available at <https://doi.org/10.5281/zenodo.11239560>.

**Table 3.** Proper motion and parallax measurements for Swift J1818.0–1607

method	$\sigma_{ij}$	$\eta_{\text{EFAC}}$	$\eta_{\delta}$	$\mu_{\alpha} \equiv \dot{\alpha} \cos \delta$	$\mu_{\delta}$	$\varpi$
				(mas yr <sup>-1</sup> )	(mas yr <sup>-1</sup> )	(mas)
least-square fitting	$\sqrt{(\sigma_{ij}^{\mathcal{R}})^2 + (\sigma_{ij}^{\mathcal{S}})^2}$	—	—	$-3.570 \pm 0.016$	$-7.723 \pm 0.035$	$0.121 \pm 0.018$
bootstrap	$\sigma_{ij}^{\mathcal{R}}$	—	—	$-3.575^{+0.018}_{-0.015}$	$-7.694^{+0.039}_{-0.038}$	$0.122^{+0.026}_{-0.023}$
bootstrap	$\sqrt{(\sigma_{ij}^{\mathcal{R}})^2 + (\sigma_{ij}^{\mathcal{S}})^2}$	—	—	$-3.572 \pm 0.015$	$-7.720^{+0.051}_{-0.050}$	$0.123^{+0.022}_{-0.020}$
Bayesian	$\sqrt{(\sigma_{ij}^{\mathcal{R}})^2 + (\eta_{\text{EFAC}} \cdot \sigma_{ij}^{\mathcal{S}})^2}$	$1.04^{+0.25}_{-0.20}$	—	$-3.571^{+0.024}_{-0.023}$	$-7.723 \pm 0.053$	$0.122 \pm 0.026$
Bayesian	$\sqrt{(\sigma_{ij}^{\mathcal{R}})^2 + (\eta'_i \cdot \sigma_{ij}^{\mathcal{S}})^2}$	$0.73^{+0.36}_{-0.31}$	$1.7^{+1.5}_{-0.7}$	$-3.572 \pm 0.019$	$-7.724^{+0.060}_{-0.063}$	$0.121^{+0.020}_{-0.021}$

$\sigma_{ij}$  stands for the total positional uncertainties, where  $i = \alpha, \delta$  refers to right ascension or declination, and  $j = 1, 2, 3, \dots$  specifies an observation.  $\eta_{\text{EFAC}}$  and  $\eta$  are the systematics-correcting factors defined in Section 4.1.  $\mu_{\alpha}$  and  $\mu_{\delta}$  represent, respectively, the right ascension and the declination component of the proper motion.  $\varpi$  denotes the parallax. The estimates at the bottom are adopted as the final results (see Section 4.1 for justifications).

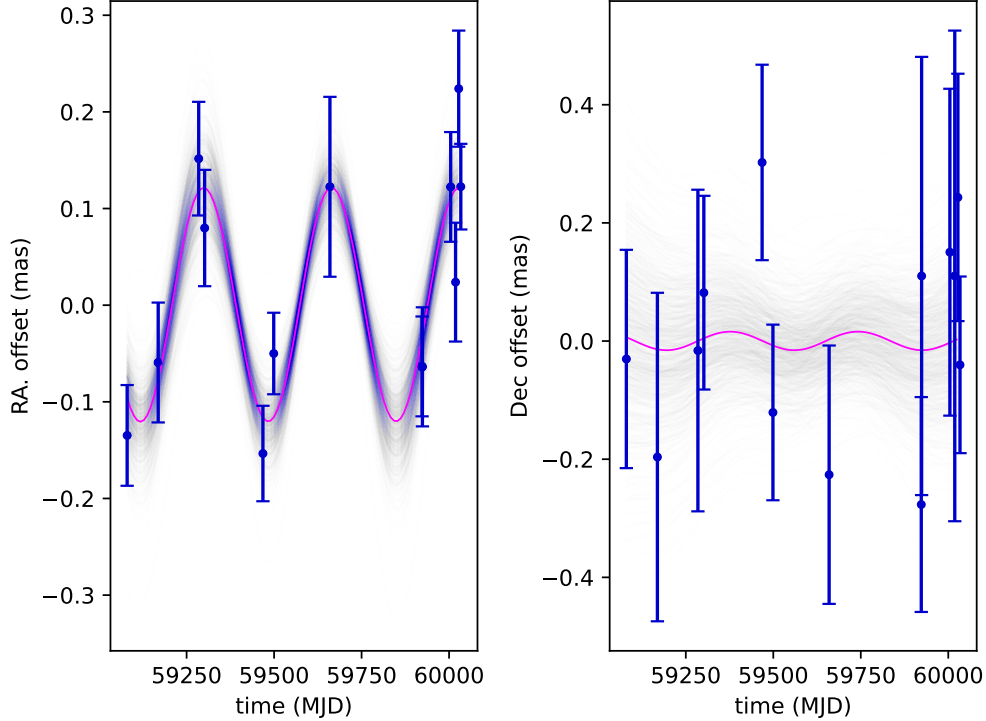


**Figure 2.** Position evolution of Swift J1818.0–1607 with the best-fit proper motion effects removed. The positional uncertainties are calculated with Equation 2, and already include the effects of the two nuisance parameters correcting the systematic errors. The inferred astrometric model is shown with the pink curve, while the overlaid Bayesian simulations visualize the uncertainty of the model.

Between the two Bayesian realizations, we expect the 2NP inference to more accurately characterize the systematics (as compared to using one nuisance parameter), at an acceptable cost (5%) of statistical significance. Therefore, we use the results of the 2NP inference for the discussions that follow in this Letter. As shown in Table 3, the 2NP Bayesian inference suggests that the one-nuisance-parameter (hereafter abbreviated as 1NP) inference overstates  $\sigma_{\alpha_j}^S$  by a factor of  $\sim 1.4$ , while underestimating  $\sigma_{\delta_j}^S$  by a factor of  $\sim 1.2$ . Accordingly, the proper motion in RA  $\mu_\alpha$  is more precise with the 2NP inference, while the uncertainty on the proper motion in declination  $\mu_\delta$  gets larger. Because the parallax effect is much more prominent in RA (than in declination), the reduction in uncertainties of the RA measurements in this approach means that higher parallax precision results from the 2NP Bayesian inference, as compared to the 1NP inference.

#### 4.2. *The absolute position of Swift J1818.0–1607*

The full astrometric model must also include the reference position of Swift J1818.0–1607. Due to the relative astrometry nature of this work, the reference position provided by any astrometric inference can only be considered as a relative position with respect to the phase calibrator(s). To derive the absolute position (of Swift J1818.0–1607) that can be compared with a position measured elsewhere (e.g., with pulsar timing), we followed the procedure described in Section 4.4 of Ding et al. (2020c), and obtained the absolute position  $18^{\text{h}}18^{\text{m}}00^{\text{s}}.193170(9), -16^{\circ}07'53''.0190(2)$  at the reference epoch of MJD 59660. Here, the positional uncertainty includes **1**) the positional uncertainties of the two reference sources, **2**) the residual first-order propagation-related systematic uncertainty, and **3**) the position offset induced by the FD-CSs of the reference sources. The absolute position is based on the calibrator positions  $18^{\text{h}}25^{\text{m}}36^{\text{s}}.532303 \pm 0.12 \text{ mas}, -17^{\circ}18'49''.84746 \pm 0.17 \text{ mas}$  and  $18^{\text{h}}05^{\text{m}}31^{\text{s}}.23753 \pm 0.26 \text{ mas}, -14^{\circ}08'44''.68657 \pm 0.44 \text{ mas}$  reported for ICRF J182536.5–171849 and ICRF J180531.2–140844, respectively, in the latest 2024a release of the Radio Fundamental Catalogue<sup>6</sup>. Thanks to the relatively high observing frequency ( $\sim 8.7 \text{ GHz}$ ) of this work, the position offset due to FDCSs is  $\lesssim 0.06 \text{ mas}$  (Sokolovsky et al. 2011), thus  $\lesssim 0.04 \text{ mas}$  in either right ascension or declination, much smaller than the  $\sim 0.8 \text{ mas}$  level at  $\sim 1.5 \text{ GHz}$  (Sokolovsky et al. 2011; Ding et al. 2020a) where most

astrometric campaigns of pulsars are carried out (e.g. Deller et al. 2019; Ding et al. 2023b).

## 5. DISTANCE & VELOCITY

The determination of both parallax and proper motion of Swift J1818.0–1607 enables us to derive its distance and the space velocity, which are desired for achieving the scientific goals outlined in Section 1. The space velocity refers to the relative velocity with respect to the stellar neighbourhood, which can be linked to the natal kick received at the NS birth. As no information of the radial velocity  $v_r$  is available, we can only constrain the space velocity tangential to the line of sight, hereafter referred to as the transverse space velocity  $v_\perp$ .

### 5.1. *The distance to Swift J1818.0–1607*

To infer a parallax-based distance normally requires a prior Galactic spatial distribution (e.g. Igoshev et al. 2016; Bailer-Jones et al. 2021), although the impact of the prior choice approaches negligible levels once the parallax is measured with  $\gtrsim 7\sigma$  significance (Lutz & Kelker 1973). With no Galactic spatial distribution available for magnetars, we instead use the Galactic spatial distribution of pulsars (“Model C”) provided by Lorimer et al. (2006). Following the procedure described in Section 6.1 of Ding et al. (2023b), we obtained the distance  $9.4_{-1.6}^{+2.0} \text{ kpc}$  to Swift J1818.0–1607. Unlike the millisecond pulsars discussed in Ding et al. (2023b), Galactic magnetars are much younger objects situated close to the Galactic plane (see Figure 1 of Ding et al. 2023a). Therefore, we adopted the original parameter “ $E$ ” (i.e., 0.18 kpc) of the “Model C” given by Lorimer et al. (2006) for the prior spatial distribution. The probability density function (PDF) and cumulative distribution function (CDF) of distance are plotted in Figure 3. For comparison, the PDF and CDF derived without assuming any prior spatial distribution are overlaid to Figure 3. We found that the use of the pulsar spatial distribution (Lorimer et al. 2006) slightly enlarges the distance estimate while reducing the skewness of the PDF. However, the impact of the prior spatial distribution (on the distance inference) is very limited thanks to the relatively high parallax significance.

### 5.2. *The transverse space velocity of Swift J1818.0–1607*

The transverse space velocity  $v_\perp$  of Swift J1818.0–1607 was estimated by the same method detailed in Section 6.2 of Ding et al. (2023b). At a Galactic latitude  $b$  of only  $-0^\circ 14'$ , the motion (and hence the velocity) of the star field surrounding Swift J1818.0–1607 can be safely approximated

<sup>6</sup> <https://astrogeo.org/>

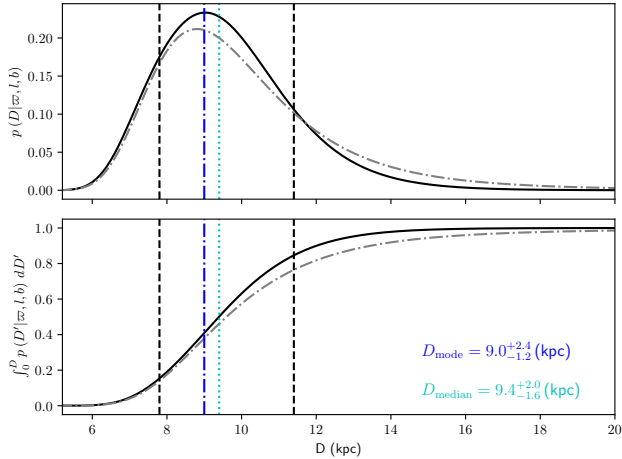


**Figure 3.** The distance  $D$  of Swift J1818.0–1607 inferred from the parallax  $\varpi$ , the Galactic longitude  $l$  and Galactic latitude  $b$  (see Section 5). The solid curves in the upper and lower panel represent, respectively, the probability density function (PDF) and the cumulative distribution function (CDF) of distance. The dashed vertical lines correspond to 0.16 and 0.84 of the CDF, and enclose the  $1\sigma$  uncertainty interval of the distance. For comparison, the PDF and CDF disregarding prior spatial distribution are shown with the dash-dotted grey curves.

by circular motion on the Galactic plane around the Galactic Center. We obtained  $v_{\perp} = 48^{+50}_{-16}$  km s $^{-1}$  for Swift J1818.0–1607.

## 6. DISCUSSIONS

This work has led to the second annual-geometric-parallax-based distance of a magnetar, which is among the largest pulsar distances measured at high significance (see the Catalogue of Pulsar Parallaxes<sup>7</sup>). According to the distance presented here, Swift J1818.0–1607 is most likely situated at the far side of the Galactic central region densely populated with stars. In addition, the  $v_{\perp}$  of Swift J1818.0–1607 is the smallest one ever determined for a magnetar (see Figure 4). These new astrometric results have several implications, which we discuss below.

### 6.1. Comparison with DM-based distances

The DM of Swift J1818.0–1607 is  $699.2(8)$  pc cm $^{-3}$  (Oswald et al. 2021). Using the `pygedm`<sup>8</sup> package (Price et al. 2021), we obtained DM-based distances  $8.0 \pm 2.0$  kpc and  $4.8 \pm 1.2$  kpc for Swift J1818.0–1607, based on, respectively, the NE2001 (Cordes & Lazio 2002) and the YMW16 model (Yao et al. 2017) —

the two latest models of Galactic free-electron distribution  $n_e$ . Here, indicative 25% fraction uncertainties are prescribed to both DM-based distances. Our new trigonometric distance  $9.4^{+2.0}_{-1.6}$  kpc agrees with and favors the NE2001 prediction, while being larger than the YMW16-model-based distance with  $\sim 2\sigma$  confidence.

### 6.2. The upper limit to the quiescent X-ray luminosity

So far, X-ray luminosities or burst fluences of Swift J1818.0–1607 have been calculated with the relatively small DM-based distances, thus being systematically under-estimated. For instance, the upper limit of the quiescent X-ray luminosity  $L_{\text{qui}}$  of Swift J1818.0–1607 is estimated to be  $5.5 \times 10^{33}$  erg s $^{-1}$  assuming the YMW16-model-based 4.8 kpc distance, which is lower than expected for a young magnetar by an order of magnitude (Esposito et al. 2020). The new trigonometric distance refines the upper limit (of the  $L_{\text{qui}}$  of Swift J1818.0–1607) to  $2.1 \times 10^{34}$  erg s $^{-1}$ , which is now more consistent with expectation ( $\gtrsim 6 \times 10^{34}$  erg s $^{-1}$ , Viganò et al. 2013; Esposito et al. 2020). Additionally, the refined  $L_{\text{qui}}$  upper limit remains lower than the spin-down luminosity of  $\sim 10^{36}$  erg s $^{-1}$  (Esposito et al. 2020), leaving it ambiguous if Swift J1818.0–1607 is mainly rotationally or magnetically powered (as questioned by Rea et al. 2012; Esposito et al. 2020).

### 6.3. The upper limit to the distance of the first scattering IISM screen

In Section 3.1, we derived the half width  $\theta_{\text{sc}} = 45 \pm 15$  mas of the angular-broadened size (of Swift J1818.0–1607) at 1.6 GHz induced by IISM scattering. In addition to the angular broadening effect, IISM may also lead to the broadening of the pulse profile of a pulsar, which can be characterized by temporal pulse broadening  $\tau_{\text{sc}}$  (Cordes et al. 1985; Cordes & Lazio 1991; Cordes 2005; Ocker et al. 2022). Assuming the IISM scattering is dominated by one thin IISM screen, the distance to the dominant IISM screen can be determined geometrically. Incorporating  $\tau_{\text{sc}} = 8.8 \pm 0.2$  ms (of Swift J1818.0–1607) at 1.6 GHz (Lower et al. 2020b) and the new distance to Swift J1818.0–1607, we calculate our distance to the dominant scattering IISM screen (in front of Swift J1818.0–1607) to be  $2.6^{+1.8}_{-0.9}$  kpc using Equation 16 of Ding et al. (2023b).

In a more realistic model, there must be multiple scattering IISM screens. In this case, we can place the upper limit  $2.6^{+1.8}_{-0.9}$  kpc to the distance of the first (closest to us) IISM screen, according to Equation 20 of Ding et al. (2023b).

### 6.4. On a proposed supernova remnant association

<sup>7</sup> <https://hosting.astro.cornell.edu/research/parallax/>

<sup>8</sup> <https://github.com/FRBs/pygedm>



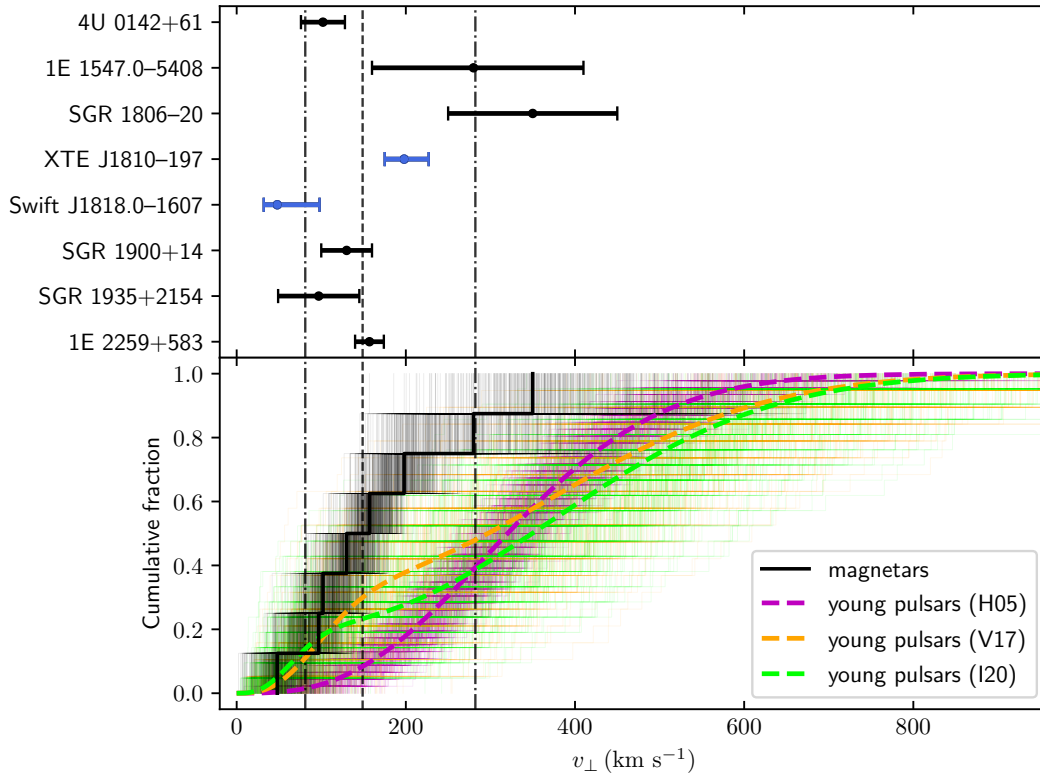


**Figure 4. Upper:** The transverse space velocities  $v_{\perp}$  of 8 magnetars, including the seven  $v_{\perp}$  estimates historically reported by Deller et al. (2012); Tendulkar et al. (2012, 2013); Ding et al. (2020c); Lyman et al. (2022). Among the 8 magnetars, proper motions are constrained for all sources with either infrared/optical (Tendulkar et al. 2012, 2013; Lyman et al. 2022) or VLBI astrometry (Helfand et al. 2007; Deller et al. 2012; Ding et al. 2020c), while model-independent parallax-based distances are determined for two magnetars (Ding et al. 2020c), for which the  $v_{\perp}$  estimates are highlighted in blue. **Lower:** The cumulative fraction of the magnetar  $v_{\perp}$  estimates is shown with a thick black stepped lines, while thin black ones based on simulations visualize the uncertainty of the cumulative fraction. For comparison, the cumulative fractions of three  $v_{\perp}$  distributions of young pulsars, converted from the respective 3-dimensional velocity distributions (Hobbs et al. 2005; Verbunt et al. 2017; Igoshev 2020), are overlaid with different colors. The colored dashed curves display the best-fit cumulative distribution functions (CDFs). The thin colored stepped lines show simulations based on the CDFs, while taking into account the uncertainties of CDF parameters. The overall  $v_{\perp}$  magnitude is estimated with Monte Carlo simulation. The 16th, 50th and 84th percentiles of the  $v_{\perp}$  simulations, marked with the vertical lines, give the estimate  $v_{\perp} = 149_{-68}^{+132}$  km s $^{-1}$ .

As mentioned in Section 1, the formation mechanism of magnetars is still under debate. It is believed that at least some Galactic magnetars were born in CCSNe, given their associations with SNRs (see the McGill Online Magnetar Catalog<sup>1</sup>, Olausen & Kaspi 2014). Therefore, searching for associated SNRs is essential for investigating magnetar formation channels. Additionally, CCSN association is important for understanding magnetar evolution, and whether they are evolutionarily connected to other NS species (e.g. XDINS, see Keane & Kramer 2008; Benli & Ertan 2016).

The low proper motion and the extraordinary youth of Swift J1818.0–1607 suggest that a putative SNR associated with Swift J1818.0–1607, if existent, must be centered around Swift J1818.0–1607. The recently discovered semi-circular radio feature around

Swift J1818.0–1607 (Ibrahim et al. 2023) serves as a prime candidate of the putative SNR associated with Swift J1818.0–1607. According to Ibrahim et al. (2023), if the semi-circular radio feature is indeed a part of an SNR, it is expected to be  $\gtrsim 8$  kpc away (from us) to have entered the full Sedov phase (Truelove & McKee 1999; Sedov 2018), which is consistent with our new magnetar distance of around 9 kpc. Therefore, the new magnetar distance sustains the interpretation that the semi-circular radio feature is the SNR associated with Swift J1818.0–1607.

#### 6.5. Revisiting the magnetar space velocity distribution

Previously, 8 magnetars have been astrometrically studied at X-rays (Kaplan et al. 2008), infrared/optical, (Tendulkar et al. 2012, 2013; Lyman et al. 2022) or ra-

dio (Helfand et al. 2007; Deller et al. 2012; Bower et al. 2015; Ding et al. 2020c), which achieved proper motion constraints for the 8 magnetars, and determined 1 significant magnetar parallax (Ding et al. 2020c). To focus on the  $v_{\perp}$  distribution of field (or isolated) magnetars, we remove SGR J1745–2900 believed to be associated with Sgr A\* (e.g. Bower et al. 2015) from the list of the magnetars. The  $v_{\perp}$  estimates reported for the remaining 7 magnetars are compiled in Figure 4.

This work obtains the second highly desired significant magnetar parallax, and leads to a robust  $v_{\perp}$  determination. With hitherto the smallest magnetar  $v_{\perp}$  added to the existing sample of 7, we revisit the magnetar  $v_{\perp}$  distribution. Given that a few  $v_{\perp}$  uncertainties are asymmetric, we estimate the overall magnetar  $v_{\perp}$  magnitude with Monte-Carlo simulations described in Section 6.2 of Ding et al. (2023b). From the  $v_{\perp}$  simulations,  $v_{\perp} = 149_{-68}^{+132}$  km s<sup>-1</sup> is estimated for the whole sample of astrometrically studied magnetars, where the median of the  $v_{\perp}$  simulations is adopted as the overall  $v_{\perp}$  estimate, and the  $v_{\perp}$  values at the 16th and the 84th percentiles of the  $v_{\perp}$  simulations define the  $1\sigma$  uncertainty interval. Assuming that the directions of the magnetar 3D space velocities  $v$  are uniformly random, it is easy to calculate that  $v \sim 4/\pi \cdot v_{\perp} = 190_{-87}^{+168}$  km s<sup>-1</sup>, which is smaller than the mean 3D velocity of young ( $\tau_c < 3$  Myr) pulsars ( $400 \pm 40$  km s<sup>-1</sup>) estimated by Hobbs et al. (2005).

Furthermore, we compare the cumulative fraction of magnetar  $v_{\perp}$  to three empirical velocity distributions of young pulsars. The three reference velocity distributions are **1**) the Maxwellian distribution with the scale parameter  $\sigma^{\text{Max}} = 265$  km s<sup>-1</sup> derived by Hobbs et al. (2005) (H05), **2**) the bimodal distribution reported in Table 4 (“Isotropic models”, “Y”) of Verbunt et al. (2017) (V17), and **3**) the bimodal distribution offered at the bottom of Table 2 of Igoshev (2020) (I20). All the three reference distributions are provided for 3-dimensional velocities  $v$ , which are converted to  $v_{\perp}$  distributions using the aforementioned relation  $v_{\perp} \sim \pi/4 \cdot v$ .

In practice, we examine the null hypothesis that the magnetar  $v_{\perp}$  sample follows a given young pulsar  $v_{\perp}$  distribution, using the Kolmogorov–Smirnov (KS) test and the Anderson–Darling (AD) test, one after another. Specifically, we simulate 8 magnetar  $v_{\perp}$  assuming normal distribution (or split normal distribution when the uncertainty is asymmetric). On the opposite side,  $N_s$  simulations are drawn from a reference distribution, where  $N_s$  is the size of the sample from which the original reference distribution is derived (see Table 4 for  $N_s$ ). We make KS/AD test with the two simulated  $v_{\perp}$  series, and record the p-value  $\zeta$  of the null hypothesis. This proce-

**Table 4.** Results of Kolmogorov–Smirnov and Anderson–Darling tests of the magnetar  $v_{\perp}$  sample against velocity distribution of young pulsars

ref. <sup>a</sup>	$N_s$	KS test		AD test	
		$\zeta$ <sup>b</sup>	$f_{\zeta < 0.05}$	$\zeta$	$f_{\zeta < 0.05}$
H05	46	$0.005_{-0.004}^{+0.018}$	95%	$0.002_{-0.001}^{+0.008}$	98%
V17	19	$0.10_{-0.09}^{+0.33}$	40%	$0.08_{-0.07}^{+0.17}$	42%
I20	21	$0.04_{-0.04}^{+0.20}$	55%	$0.04_{-0.04}^{+0.18}$	54%

<sup>a</sup>The reference velocity distributions of young pulsars, each derived from a velocity sample of sample size  $N_s$ , are provided by Hobbs et al. (2005), Verbunt et al. (2017), and Igoshev (2020).

<sup>b</sup> $\zeta$  and  $f_{\zeta < 0.05}$  denote, respectively, the p-value of the null hypothesis (that the magnetar  $v_{\perp}$  sample follows the reference distribution), and the fraction of 10,000 simulations resulting in  $\zeta < 0.05$ .

cedure is repeated 10,000 times, which leads to 10,000  $\zeta$ . The results of the KS/AD tests are provided in Table 4. We find significant evidence suggesting that the magnetar  $v_{\perp}$  sample does not follow the unimodal young pulsar velocity distribution proposed by H05, with at least 95% of the simulations rendering  $\zeta < 0.05$ . On the other hand, there is no sufficient evidence for ruling out the possibility that the magnetar  $v_{\perp}$  sample follows either bimodal young pulsar velocity distribution that is derived from a much smaller but more accurate velocity sample compared to H05. The cumulative fractions of the magnetar  $v_{\perp}$  sample and the aforementioned young pulsar  $v_{\perp}$  distribution are illustrated in Figure 4, overlaid with the related simulations.

Additionally, the magnetar  $v_{\perp}$  sample can, in principle, be used to probe the modality of the underlying  $v_{\perp}$  distribution with, e.g., Hartigan’s dip test (Hartigan & Hartigan 1985; Hartigan 1985). Following the Monte-Carlo procedure described in Section 7.2.3 of Ding et al. (2024), we obtain the mean dip-test p-value of 0.7, indicating no multimodality of the underlying  $v_{\perp}$  distribution. When assuming magnetar velocities follow the V17 and I20 young pulsar distributions, we find out with simulation that, respectively,  $\sim 1590$  and  $\sim 130$  additional magnetar  $v_{\perp}$  determinations are required to rule out unimodality at 90% confidence.

Finally, it is important to note that the current magnetar  $v_{\perp}$  sample might be biased against low-velocity magnetars due to relatively low spatial resolution of optical/infrared facilities. This bias will be reduced with increasing time baseline of astrometry. Additionally, the magnetar sample is biased towards brighter magnetars

that tend to be closer ( $\lesssim 10$  kpc) to us, though its impact on  $v_{\perp}$  is likely limited.

## 7. SUMMARY AND FUTURE PROSPECTS

In this work, we observed the fastest-spinning magnetar Swift J1818.0–1607 from April 2020 to March 2023 with the VLBA, in order to determine its astrometric information. To suppress propagation-related systematic errors, the 1D interpolation strategy was adopted. Using a Bayesian framework, we derived (from the measured position series) precise proper motion and parallax for Swift J1818.0–1607, along with two nuisance parameters that correct the systematic errors. The parallax  $\varpi = 0.12 \pm 0.02$  mas is the second magnetar parallax, and is among the smallest pulsar parallaxes ever measured; it corresponds to the trigonometric distance  $d = 9.4_{-1.6}^{+2.0}$  kpc, locating Swift J1818.0–1607 at the far side of the Galactic central region. The parallax determination demonstrates that robust and precise trigonometric distance up to  $\sim 10$  kpc can be determined for Galactic magnetars, which holds the key to substantially reducing distance-related errors (including systematic errors) in  $v_{\perp}$ .

With the trigonometric distance of Swift J1818.0–1607, the upper limit to the quiescent X-ray luminosity reported by Esposito et al. (2020) is refined to  $2.1 \times 10^{34}$  erg s $^{-1}$ , which is more consistent with expectation (Viganò et al. 2013). Combining the pulse broadening  $\tau_{sc}$  measured by Lower et al. (2020b), the trigonometric distance, and the angular broadening of Swift J1818.0–1607, we calculate the upper limit  $2.6_{-0.9}^{+1.8}$  kpc of our distance to the closest scattering IISM screen in front of Swift J1818.0–1607. In addition, the new magnetar distance agrees with the indicative distance constraint  $\gtrsim 8$  kpc of a tentative SNR around Swift J1818.0–1607, thus sustaining the interpretation that the semi-circular radio feature discovered around Swift J1818.0–1607 is an SNR associated with Swift J1818.0–1607 (Ibrahim et al. 2023).

Incorporating the proper motion of Swift J1818.0–1607 with  $d$ , we obtain a low transverse space velocity  $v_{\perp} = 48_{-16}^{+50}$  km s $^{-1}$ . With the enriched  $v_{\perp}$  sample of 8 astrometrically studied magnetars, we find that the magnetar  $v_{\perp}$  sample is unlikely to reconcile with the unimodal young pulsar velocity distribution reported by Hobbs et al. (2005), while being marginally consistent with the more recent bimodal young pulsar velocity

distributions derived from VLBI results (Verbunt et al. 2017; Igoshev 2020).

Looking into the future, multi-wavelength high-sensitivity observations towards the sky region around Swift J1818.0–1607 will constrain the amount of matter blown into the space at the birth of Swift J1818.0–1607, hence probing the formation channel of Swift J1818.0–1607. To further refine the magnetar  $v_{\perp}$  distribution, more astrometric measurements of magnetars are desired, which is ultimately limited by the number of identified magnetars in the Galaxy.

## ACKNOWLEDGEMENTS

We appreciate the useful comments from the anonymous reviewer, which have well improved the quality of this paper. HD acknowledges the EACOA Fellowship awarded by the East Asia Core Observatories Association. This work is mainly based on observations with the Very Long Baseline Array (VLBA), which is operated by the National Radio Astronomy Observatory (NRAO). The NRAO is a facility of the National Science Foundation operated under cooperative agreement by Associated Universities, Inc. This work made use of the Swinburne University of Technology software correlator, developed as part of the Australian Major National Research Facilities Programme and operated under license. HD thanks the NRAO VLBA observational support staff (Paul and Anthony) for generous efforts in support of pulsar gating at correlation, including multiple re-correlation passes when required. Murriyang, the Parkes radio telescope, is part of the Australia Telescope National Facility (<https://ror.org/05qajvd42>) which is funded by the Australian Government for operation as a National Facility managed by CSIRO. We acknowledge the Wiradjuri people as the Traditional Owners of the Observatory site.

*Facilities:* Very Long Baseline Array, Murriyang/Parkes radio telescope

*Software:* `astropy` (Astropy Collaboration et al. 2013, 2018, 2022), `numpy` (Harris et al. 2020), `scipy` (Virtanen et al. 2020), `matplotlib` (Hunter 2007), `sterne.py` (Ding et al. 2021), `corner.py` (Foreman-Mackey 2016), `bilby` (Ashton et al. 2019), `ParselTongue` (Kettenis et al. 2006), `AIPS` (Greisen 2003), `DIFMAP` (Shepherd et al. 1994), `corner.py` (Foreman-Mackey 2016), `pygedm` (Price et al. 2021), `pmpar`<sup>9</sup>, `psrqpy` (Pitkin 2018)

<sup>9</sup>

<https://github.com/walterfb/pmpar>

## REFERENCES

- Ai, S., & Zhang, B. 2021, *ApJL*, 915, L11
- Andersen, B. C., Bandura, K. M., Bhardwaj, M., et al. 2020, *Nature*, 587, 54, doi: [10.1038/s41586-020-2863-y](https://doi.org/10.1038/s41586-020-2863-y)
- Ashton, G., Hübner, M., Lasky, P. D., et al. 2019, *ApJS*, 241, 27, doi: [10.3847/1538-4365/ab06fc](https://doi.org/10.3847/1538-4365/ab06fc)
- Astropy Collaboration, Robitaille, T. P., Tollerud, E. J., et al. 2013, *A&A*, 558, A33, doi: [10.1051/0004-6361/201322068](https://doi.org/10.1051/0004-6361/201322068)
- Astropy Collaboration, Price-Whelan, A. M., Sipőcz, B. M., et al. 2018, *AJ*, 156, 123, doi: [10.3847/1538-3881/aabc4f](https://doi.org/10.3847/1538-3881/aabc4f)
- Astropy Collaboration, Price-Whelan, A. M., Lim, P. L., et al. 2022, *ApJ*, 935, 167, doi: [10.3847/1538-4357/ac7c74](https://doi.org/10.3847/1538-4357/ac7c74)
- Bailer-Jones, C., Rybizki, J., Fouesneau, M., Demleitner, M., & Andrae, R. 2021, *AJ*, 161, 147, doi: [10.3847/1538-3881/abd806](https://doi.org/10.3847/1538-3881/abd806)
- Bailes, M., Bassa, C., Bernardi, G., et al. 2021, *MNRAS*, 503, 5367
- Benli, O., & Ertan, Ü. 2016, *MNRAS*, 457, 4114
- Bochenek, C. D., Ravi, V., Belov, K. V., et al. 2020, *Nature*, 587, 59
- Borkowski, K. J., & Reynolds, S. P. 2017, *ApJ*, 846, 13
- Bower, G. C., Deller, A., Demorest, P., et al. 2014, *ApJL*, 780, L2
- . 2015, *ApJ*, 798, 120
- Camilo, F., Reynolds, J., Johnston, S., Halpern, J., & Ransom, S. 2008, *ApJ*, 679, 681
- Camilo, F., Cognard, I., Ransom, S., et al. 2007, *ApJ*, 663, 497
- Champion, D., Cognard, I., Cruces, M., et al. 2020, *MNRAS*, 498, 6044
- Cordes, J., Weisberg, J., & Boriakoff, V. 1983, *ApJ*, 268, 370
- . 1985, *ApJ*, 288, 221
- Cordes, J. M. 2005, in *Low Frequency Astrophysics from Space: Proceedings of an International Workshop Held in Crystal City, Virginia, USA, on 8 and 9 January 1990*, Springer, 165–174
- Cordes, J. M., & Lazio, T. J. 1991, *ApJ*, 376, 123
- Cordes, J. M., & Lazio, T. J. W. 2002, arXiv preprint [astro-ph/0207156](https://arxiv.org/abs/astro-ph/0207156)
- Deller, A., Camilo, F., Reynolds, J., & Halpern, J. 2012, *ApJL*, 748, L1
- Deller, A. T., Briskin, W. F., Phillips, C. J., et al. 2011, *PASP*, 123, 275, doi: [10.1086/658907](https://doi.org/10.1086/658907)
- Deller, A. T., Goss, W. M., Briskin, W. F., et al. 2019, *ApJ*, 875, 100, doi: [10.3847/1538-4357/ab11c7](https://doi.org/10.3847/1538-4357/ab11c7)
- Dessart, L., Burrows, A., Livne, E., & Ott, C. 2007, *ApJ*, 669, 585
- Ding, H. 2022, PhD thesis, Swinburne University of Technology. <https://arxiv.org/abs/2212.08881>
- Ding, H., & Deller, A. 2024, *dingswin/sterne: v2.1.1*, Zenodo, doi: [10.5281/ZENODO.11239560](https://doi.org/10.5281/ZENODO.11239560)
- Ding, H., Deller, A., Lower, M., & Shannon, R. 2023a, *Proceedings of the International Astronomical Union*, 16, 271, doi: [10.1017/S1743921322000321](https://doi.org/10.1017/S1743921322000321)
- Ding, H., Deller, A. T., Fonseca, E., et al. 2021, *ApJL*, 921, L19, doi: [10.3847/2041-8213/ac3091](https://doi.org/10.3847/2041-8213/ac3091)
- Ding, H., Deller, A. T., Freire, P., et al. 2020a, *ApJ*, 896, 85, doi: [10.3847/1538-4357/ab8f27](https://doi.org/10.3847/1538-4357/ab8f27)
- Ding, H., Deller, A. T., Lower, M. E., & Shannon, R. M. 2020b, *ATel*, 14005, 1
- Ding, H., Deller, A. T., Swiggum, J. K., et al. 2024, arXiv preprint [arXiv:2405.03914](https://arxiv.org/abs/2405.03914)
- Ding, H., Deller, A. T., Lower, M. E., et al. 2020c, *MNRAS*, 498, 3736, doi: [10.1093/mnras/staa2531](https://doi.org/10.1093/mnras/staa2531)
- Ding, H., Deller, A. T., Stappers, B. W., et al. 2023b, *MNRAS*, 519, 4982, doi: [10.1093/mnras/stac3725](https://doi.org/10.1093/mnras/stac3725)
- Doi, A., Fujisawa, K., Habe, A., et al. 2006, *PASJ*, 58, 777
- Efron, B., & Tibshirani, R. J. 1994, *An introduction to the bootstrap* (Chapman and Hall/CRC)
- Enoto, T., Sakamoto, T., Younes, G., et al. 2020, *ATel*, 13551, 1
- Esposito, P., Rea, N., Borghese, A., et al. 2020, *ApJL*, 896, L30
- Fomalont, E. B., & Kopeikin, S. M. 2003, *ApJ*, 598, 704
- Foreman-Mackey, D. 2016, *The Journal of Open Source Software*, 1, 24, doi: [10.21105/joss.00024](https://doi.org/10.21105/joss.00024)
- Fryer, C., Benz, W., Herant, M., & Colgate, S. A. 1999, *ApJ*, 516, 892
- Gaensler, B. 2014, *GRB Coordinates Network*, 16533, 1
- Gaensler, B., & Chatterjee, S. 2008, *GRB Coordinates Network*, 8149, 1
- Gelfand, J. D., & Gaensler, B. 2007, *ApJ*, 667, 1111
- Giacomazzo, B., & Perna, R. 2013, *ApJL*, 771, L26
- Goodman, J., & Narayan, R. 1989, *MNRAS*, 238, 995
- Greisen, E. W. 2003, in *Astrophysics and Space Science Library*, Vol. 285, *Information Handling in Astronomy - Historical Vistas*, ed. A. Heck (Springer), 109, doi: [10.1007/0-306-48080-8\\_7](https://doi.org/10.1007/0-306-48080-8_7)
- Harris, C. R., Millman, K. J., Van Der Walt, S. J., et al. 2020, *Nature*, 585, 357
- Hartigan, J. A., & Hartigan, P. M. 1985, *The annals of Statistics*, 70
- Hartigan, P. 1985, *Journal of the Royal Statistical Society. Series C (Applied Statistics)*, 34, 320
- Helfand, D. J., Chatterjee, S., Briskin, W. F., et al. 2007, *ApJ*, 662, 1198, doi: [10.1086/518028](https://doi.org/10.1086/518028)



- Heyl, J. S., & Kulkarni, S. 1998, *ApJ*, 506, L61
- Hobbs, G., Lorimer, D., Lyne, A., & Kramer, M. 2005, *MNRAS*, 360, 974
- Hunter, J. D. 2007, *Computing in science & engineering*, 9, 90
- Ibrahim, A., Borghese, A., Rea, N., et al. 2023, *ApJ*, 943, 20
- Igoshev, A., Verbunt, F., & Cator, E. 2016, *Astronomy & Astrophysics*, 591, A123
- Igoshev, A. P. 2020, *MNRAS*, 494, 3663
- Kaplan, D., Chatterjee, S., Hales, C., Gaensler, B., & Slane, P. 2008, *ApJ*, 137, 354
- Keane, E. F., & Kramer, M. 2008, *MNRAS*, 391, 2009
- Kettenis, M., van Langevelde, H. J., Reynolds, C., & Cotton, B. 2006, in *Astronomical Society of the Pacific Conference Series*, Vol. 351, *Astronomical Data Analysis Software and Systems XV*, ed. C. Gabriel, C. Arviset, D. Ponz, & S. Enrique, 497
- Klose, S., Henden, A., Geppert, U., et al. 2004, *ApJ*, 609, L13
- Lipunov, V., & Postnov, K. 1985, *A&A*, 144, L13
- Lorimer, D., Faulkner, A., Lyne, A., et al. 2006, *MNRAS*, 372, 777
- Lower, M. E., Johnston, S., Shannon, R. M., Bailes, M., & Camilo, F. 2020a, *MNRAS*
- Lower, M. E., Shannon, R. M., Johnston, S., & Bailes, M. 2020b, *ApJL*, 896, L37
- Lutz, T. E., & Kelker, D. H. 1973, *PASP*, 85, 573, doi: [10.1086/129506](https://doi.org/10.1086/129506)
- Lyman, J., Levan, A., Wiersema, K., et al. 2022, *ApJ*, 926, 121
- Macquart, J.-P., & Koay, J. Y. 2013, *ApJ*, 776, 125
- Mannings, A. G., Fong, W.-f., Simha, S., et al. 2021, *ApJ*, 917, 75
- Margalit, B., Berger, E., & Metzger, B. D. 2019, *ApJ*, 886, 110
- Ocker, S. K., Cordes, J. M., Chatterjee, S., & Gorsuch, M. R. 2022, *ApJ*, 934, 71
- Olausen, S. A., & Kaspi, V. M. 2014, *ApJS*, 212, 6, doi: [10.1088/0067-0049/212/1/6](https://doi.org/10.1088/0067-0049/212/1/6)
- Oswald, L., Karastergiou, A., Posselt, B., et al. 2021, *MNRAS*, 504, 1115
- Pitkin, M. 2018, arXiv preprint arXiv:1806.07809
- Price, D. C., Flynn, C., & Deller, A. 2021, *PASA*, 38, e038
- Rajwade, K., Stappers, B., Lyne, A., et al. 2022, *MNRAS*, 512, 1687
- Rea, N., Pons, J. A., Torres, D. F., & Turolla, R. 2012, *ApJL*, 748, L12
- Ruiter, A., Ferrario, L., Belczynski, K., et al. 2019, *MNRAS*, 484, 698
- Schneider, F. R., Ohlmann, S. T., Podsiadlowski, P., et al. 2019, *Nature*, 574, 211
- Sedov, L. I. 2018, *Similarity and dimensional methods in mechanics* (CRC press)
- Shenar, T., Wade, G. A., Marchant, P., et al. 2023, *Science*, 381, 761
- Shepherd, M. C., Pearson, T. J., & Taylor, G. B. 1994, in *BAAS*, Vol. 26, *Bulletin of the American Astronomical Society*, 987–989
- Sherman, M. B., Ravi, V., El-Badry, K., et al. 2024, *MNRAS*, stae1289
- Sokolovsky, K. V., Kovalev, Y. Y., Pushkarev, A. B., & Lobanov, A. P. 2011, *A&A*, 532, A38, doi: [10.1051/0004-6361/201016072](https://doi.org/10.1051/0004-6361/201016072)
- Sun, H., Li, Y., Zhang, B.-B., et al. 2019, *ApJ*, 886, 129
- Tendulkar, S. P., Cameron, P. B., & Kulkarni, S. R. 2012, *ApJ*, 761, 76
- . 2013, *ApJ*, 772, 31
- Thompson, C., & Duncan, R. C. 1995, *MNRAS*, 275, 255
- Torne, P., Liu, K., Cognard, I., et al. 2020, *ATel*, 14001, 1
- Truelove, J. K., & McKee, C. F. 1999, *ApJS*, 120, 299
- Vasisht, G., & Gotthelf, E. 1997, *ApJL*, 486, L129
- Verbunt, F., Igoshev, A., & Cator, E. 2017, *A&A*, 608, A57, doi: [10.1051/0004-6361/201731518](https://doi.org/10.1051/0004-6361/201731518)
- Viganò, D., Rea, N., Pons, J. A., et al. 2013, *MNRAS*, 434, 123
- Virtanen, P., Gommers, R., Oliphant, T. E., et al. 2020, *Nature Methods*, 17, 261, doi: [10.1038/s41592-019-0686-2](https://doi.org/10.1038/s41592-019-0686-2)
- Xue, Y., Zheng, X., Li, Y., et al. 2019, *Nature*, 568, 198
- Yao, J. M., Manchester, R. N., & Wang, N. 2017, *ApJ*, 835, 29, doi: [10.3847/1538-4357/835/1/29](https://doi.org/10.3847/1538-4357/835/1/29)